

# Interwoven Nanowire Based On-Chip Asymmetric Microsupercapacitor with High Integrability, Areal Energy, and Power Density

Wei Yang, Yuxuan Zhu, Zhuofei Jia, Liang He,\* Lin Xu, Jiashen Meng, Muhammad Tahir, Zixin Zhou, Xuewen Wang,\* and Liqiang Mai\*

On-chip microsupercapacitors (MSC) with facile fabrication procedures, high integration design, and superior performance are desired as an energy storage device for microelectronics. Hence, a novel procedure is proposed to fabricate an asymmetric microsupercapacitor (AMSC), employing interwoven nanowire (NW) network electrodes of poly(3,4-ethylenedioxythiophene) coated titanium oxynitride (P-TiON) and vanadium nitride (VN) NW as a cathode and an anode, respectively. The interwoven NWs with a high mass loading offer a sufficient electrochemical reaction area and rapid electron/ion transport pathway, delivering superior energy and power densities. With the LiCl/polyvinyl alcohol electrolyte, the assembled P-TiON/VN AMSC can achieve a wide voltage window from 0 to 1.8 V with an excellent areal capacitance of  $72 \text{ mF cm}^{-2}$ , a high areal energy density of  $32.4 \mu\text{Wh cm}^{-2}$  (at  $0.9 \text{ mW cm}^{-2}$ ), an outstanding power density of  $45 \text{ mW cm}^{-2}$  (at  $21.9 \mu\text{Wh cm}^{-2}$ ), and a good cycling performance. Furthermore, the substrate-free electrodes exhibit outstanding integrability, and the system on one printed circuit board including two AMSCs in series and a LED demonstrates excellent practicability.

microdevices/systems, the miniaturized on-chip energy storage devices are highly desirable for applications in microscale wireless sensors, intelligent network nodes, implantable medical devices, etc.<sup>[1,2]</sup> Compared with microbatteries, the microsupercapacitors (MSCs) have a much higher power density and a longer operating lifetime. However, the relatively low energy density greatly limits the applications of MSCs.<sup>[3]</sup> Therefore, the main strategies to enhance the areal energy density ( $E$ ) are extending the working voltage ( $V$ ) and improving the areal capacitance ( $C$ ) according to the equation of  $E = 1/2 CV^2$ . To realize high-performance MSCs, two approaches are widely adopted: 1) rationally designing asymmetric construction for MSCs to improve the working voltage;<sup>[4]</sup> 2) optimizing microstructure of electrodes to achieve high mass loading of active materials with sufficient electron/ion transport pathway within a limited footprint area.<sup>[3]</sup>

The miniaturization of microdevices has made great progress in developing the micro-sized electronic components with high-density integration. As the critical component of

3D micro/nanostructures have been widely employed as high mass loading electrodes for MSCs.<sup>[1,5]</sup> Until now, various 3D structured microelectrodes have been reported, such as inverted opal structure,<sup>[6,7]</sup> layer-by-layer stacked structure,<sup>[8,9]</sup> pillar array,<sup>[10,11]</sup> microtubular,<sup>[12]</sup> etc. These 3D nanostructured microelectrodes have high available surface area, and bicontinuous electron/ion pathways. Thus, the convenient processes to construct 3D nanostructured microelectrodes are highly required, especially for large-scale integrated MSCs, which is the critical issue of commercialization.<sup>[13,14]</sup> To the best of our knowledge, electrodeposition (EDP),<sup>[15,16]</sup> electrophoresis (EP),<sup>[17]</sup> ink coating,<sup>[18]</sup> laser patterning,<sup>[19]</sup> chemical vapor deposition (CVD) growth,<sup>[20]</sup> etc., have been employed as fabrication processes of on-chip MSCs. Among them, EP could assemble active nanomaterials on the micro current collector directly. Although, MSCs fabricated by EP could achieve high power density, their low mass loading of active materials extremely limits their energy density.<sup>[17,21]</sup> Among various active materials, nanowires (NWs) have 1D morphology with a variety of physical and chemical advantages for energy storage applications, including direct current pathways, large surface area, high volume accommodation, and high mechanical reliability.<sup>[22,23]</sup> NWs with these unique features are greatly suitable and highly promising in constructing network structured electrodes of

W. Yang, Y. X. Zhu, Z. F. Jia, Prof. L. He, Prof. L. Xu, J. S. Meng, M. Tahir, Z. X. Zhou, Prof. L. Q. Mai  
State Key Laboratory of Advanced Technology  
for Materials Synthesis and Processing  
Wuhan University of Technology  
Wuhan 430070, China  
E-mail: hel@whut.edu.cn; mlq518@whut.edu.cn

Dr. L. He  
Department of Materials Science and NanoEngineering  
Rice University  
Houston, TX 77005, USA

Prof. X. W. Wang  
International School of Materials Science and Engineering  
Wuhan University of Technology  
Wuhan 430070, P. R. China  
E-mail: xwwang@whut.edu.cn

Prof. X. W. Wang, Prof. L. Q. Mai  
Foshan Xianhu Laboratory of the Advanced Energy Science and  
Technology, Guangdong Laboratory  
Xianhu Hydrogen Valley  
Foshan 528200, P. R. China

 The ORCID identification number(s) for the author(s) of this article can be found under <https://doi.org/10.1002/aenm.202001873>.

DOI: 10.1002/aenm.202001873

MSCs to achieve large specific surface area, rapid electron/ion transport pathways, and high mass loading of active materials.

As an emerging high-performance electrode material of supercapacitors, metal nitrides with superb electrical conductivity and sustainability have aroused great attention.<sup>[24–26]</sup> As a typical transition metal nitride, titanium nitride (TiN) has fascinating potential to be employed as the MSC electrode, which has an outstanding electrical conductivity of  $3.7 \times 10^6 \text{ S m}^{-1}$ .<sup>[24,26]</sup> TiN NWs exhibit excellent electrochemical performance, benefiting from the outstanding electrical conductivity, short ion diffusion pathway, and large specific surface area, which are widely applied as the active material of energy storage devices. However, the capacitance of TiN is relatively low ( $\approx 150 \text{ F g}^{-1}$ ) and found to be easily oxidized in aqueous solutions.<sup>[26,27]</sup> Hence, it is an effective way to enhance performance through favorable coatings.<sup>[26]</sup> Owing to the relatively high capacitance ( $210 \text{ F g}^{-1}$ ), superior electrical conductivity ( $>550 \text{ S cm}^{-1}$ ), wide potential window, and high electrochemical stability,<sup>[28]</sup> poly(3,4-ethylenedioxythiophene) (PEDOT) is commonly applied as a coating layer for active materials, including  $\text{MnO}_2$ ,<sup>[29]</sup> carbon nanotube (CNT),<sup>[15]</sup> and  $\text{V}_2\text{O}_5$ ,<sup>[30]</sup> etc. As another transition metal nitride, vanadium nitride (VN) also has excellent electrical conductivity of  $1.67 \times 10^6 \text{ S m}^{-1}$ , widely applied as the supercapacitor electrode, due to its large specific capacitance of  $1340 \text{ F g}^{-1}$  and suitable negative working potential lower than  $-1 \text{ V}$ .<sup>[31]</sup> Furthermore, the VN derived from  $\text{VO}_x$  by ammonia ( $\text{NH}_3$ ) annealing is able to form porous structure and achieve outstanding electrochemical performance. Recently, various porous VN NW electrodes have been reported, for instance, freestanding mesoporous VN/CNT electrode,<sup>[32]</sup> porous VN NW electrode@carbon cloth,<sup>[31]</sup> coaxial fiber-shaped supercapacitor,<sup>[33]</sup> etc. The advantages of VN NWs are highly presented in these reported results and ultrahigh electrochemical performances are obtained. Nevertheless, high mass loading of metal-nitride NW microelectrodes is difficult to obtain via most existing fabrication technologies of MSCs, due to the nitridation at ultrahigh temperature, the high aspect ratio of NWs and the narrow gap between electrodes, greatly hindering the manufacture of metal nitride NWs based MSC.<sup>[15,18,34]</sup> Additionally, a one-chip microsystem, containing MSCs and energy-consuming components, is rarely fabricated by existing bottom-up MSC procedures, whereas the external circuits are required to connect these components.<sup>[35]</sup> Otherwise, the selection of energy-consuming components is greatly limited by the fabrication processes of MSC in multifunctional chips which incorporate the above two components, especially the MSCs by wet electrochemistry method,<sup>[6]</sup> high-temperature processing,<sup>[36]</sup> etc. Therefore, developing a novel method that effectively takes advantage of metal nitride NWs is a promising way to exploit MSCs with outstanding electrochemical performance, and superior integration.

Herein, we demonstrate an all-solid-state asymmetric micro-supercapacitor (AMSC) with PEDOT coated titanium oxynitride (TiON) NW network cathode and VN NW network anode. In our strategy, the  $\text{H}_2\text{Ti}_3\text{O}_7$  and  $\text{VO}_x$  NWs were synthesized through facile hydrothermal methods.<sup>[31,37]</sup> The dense and homogeneous NW network was formed on commercial substrate-free interdigital Ti current collectors by EP process, then the  $\text{H}_2\text{Ti}_3\text{O}_7$  and  $\text{VO}_x$  NW network microelectrodes were annealed in  $\text{NH}_3$  flow to achieve TiON and VN NW network microelectrodes, respec-

tively. TiON NW microelectrode coated with PEDOT (denote as P-TiON) was fabricated by EDP method and employed as the cathode of AMSC, and the VN NW microelectrode is employed as the anode of AMSC. These highly facile and practicable methods are able to achieve substrate-free microelectrodes and capable of integrating on chip with other components. As another significant advantage, the highly electrical conductive NW network offers ultrafast electron transfer pathways, the dense space in the network which delivers sufficient ion migration pathways, and the large specific surface area which is capable of obtaining high areal capacitance. Benefitting from such unique 3D network structure and asymmetric design, the P-TiON/VN AMSC with LiCl/polyvinyl alcohol (PVA) electrolyte delivers a wide voltage window of 0 to 1.8 V, an excellent areal capacitance of  $72 \text{ mF cm}^{-2}$ , a high areal energy density of  $32.4 \mu\text{Wh cm}^{-2}$  (at  $0.9 \text{ mW cm}^{-2}$ ), and a high areal power density of  $45 \text{ mW cm}^{-2}$  (at  $21.9 \mu\text{Wh cm}^{-2}$ ).

The fabrication process of P-TiON/VN AMSC is illustrated in **Figure 1**. The fabrication processes of VN and P-TiON NW microelectrodes are exhibited in Figures 1a,b, respectively. First, the synthesized  $\text{H}_2\text{Ti}_3\text{O}_7$  and  $\text{VO}_x$  NWs were dispersed in alcohol, separately. Then,  $\text{Mg}(\text{NO}_3)_2$  was added into these two suspensions as a surfactant to render the NWs being positively charged,<sup>[38]</sup> and the uniformly dispersed NWs in suspension were achieved. Second, EP deposition was conducted by employing interdigital Ti current collector (Figure S1a–d, Supporting Information) as the negative electrode and Pt foil as the positive electrode. During this process, a constant voltage from a direct current stabilized power supply was applied. Afterward, NWs were moistened with alcohol and fluffy covered on the Ti current collector. After drying, the continuous films assembled by high-density NW network were obtained. Third, after annealing  $\text{H}_2\text{Ti}_3\text{O}_7$  and  $\text{VO}_x$  NW microelectrodes in  $\text{NH}_3$  flow, TiON and VN NW microelectrodes were achieved. P-TiON was fabricated through coating PEDOT on the 3D TiON network by EDP method. Finally, P-TiON and VN NW microelectrodes were bonded on a printed circuit board (PCB) as the cathode and anode, respectively. The assembly process is exhibited in Figure S2, Supporting Information (this manual process could be replaced by mechanized assembly in further industrialization). Benefitting from this assembly process, the microelectrodes are capable of being applied in some flexible instruments by one-point connection with substrate (Figure S3, Supporting Information), and the microelectrodes were also bonded on a polyethylene terephthalate (PET) substrate as a wearable bangle. After assembling with LiCl/PVA electrolyte and standing for a few hours, the all-solid-state P-TiON/VN AMSC was assembled (Figure 1c). For a long period serviceability, the P-TiON/VN AMSC with packing is also achieved by covering a polyethylene (PE) film on the gel electrolyte and sealing the edge of PE film with a small amount of binder (Figure S4, Supporting Information).

**Figure 2** exhibits the scanning electron microscopy (SEM) images of TiON, P-TiON, and VN NW microelectrodes. The Ti interdigital current collector is covered by TiON NWs with a homogenous morphology, and the interspace between fine fingers of TiON NW microelectrode is reserved well (Figure 2a). Meanwhile, the color of the TiON electrode's current collector turned golden, similar to a common color of TiN film,<sup>[39]</sup>

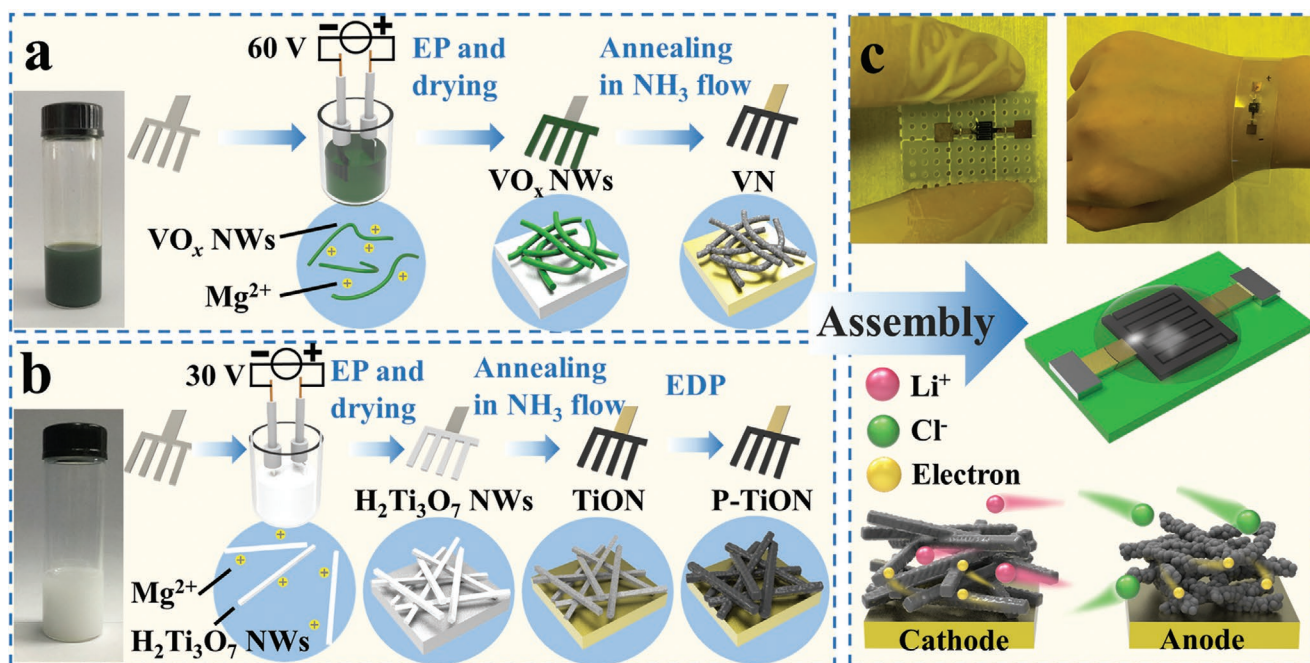


**Figure 1.** Schematic of the fabrication processes of interdigital NW network microelectrodes of a) VN electrode, b) P-TiON electrode, and c) the optical images, assembly schematic, and working principle of P-TiON/VN AMSC.

indicating sufficient nitridation of the electrode (Figure 2a, inset). As shown in Figure 2b, porous NWs are interwoven together to form a dense network structure. With PEDOT coating, the NW network structure and the finely patterned fingers are well reserved, as shown in Figure 2c and the inset. The 3D porous TiON NWs framework is completely coated with a layer of PEDOT, and the PEDOT film connects with adjacent

NWs, forming a continuous PEDOT coating layer (Figure 2d). One finger of interdigital microelectrode covered by VN NWs is also exhibited (Figure 2e). The optical image of VN interdigital microelectrode indicates its fine morphology (inset of Figure 2e). The wrinkled surface of the VN electrode is constructed by dense interwoven NWs, and the high-magnification SEM image of VN NWs clearly shows the porous morphology

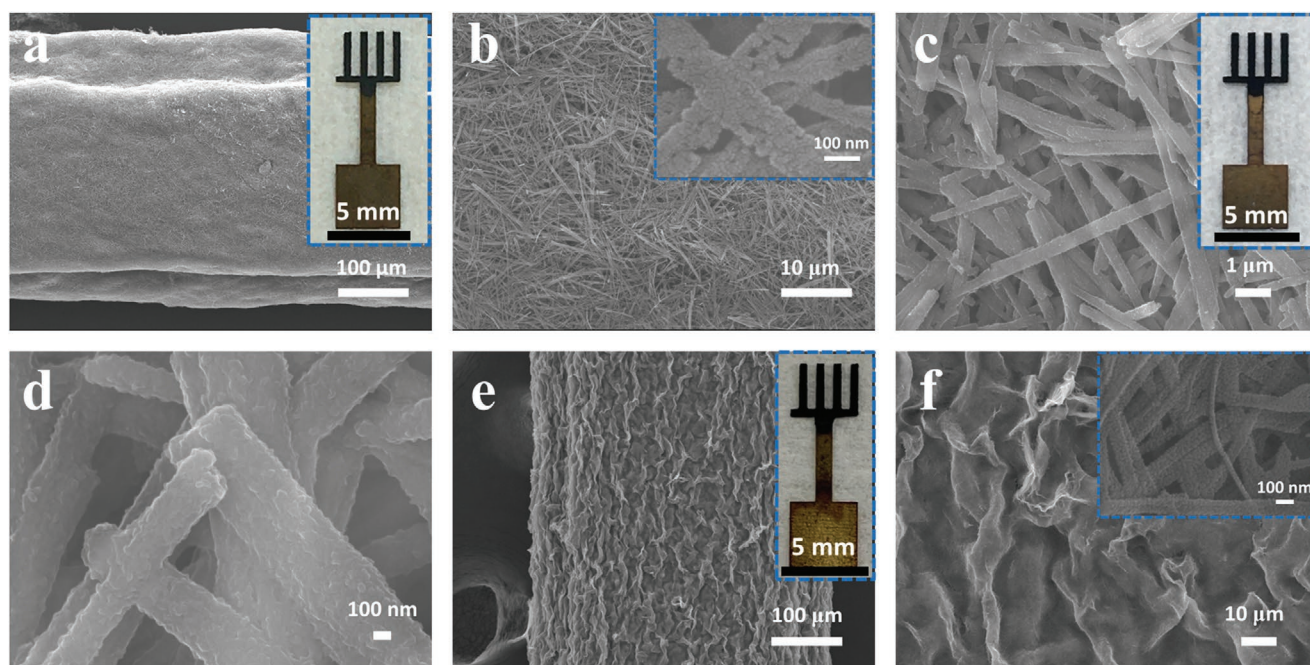


**Figure 2.** SEM images of the surfaces and optical images of a,b) TiON NW network electrode, c,d) P-TiON NW network electrode, e,f) VN NW network electrode.

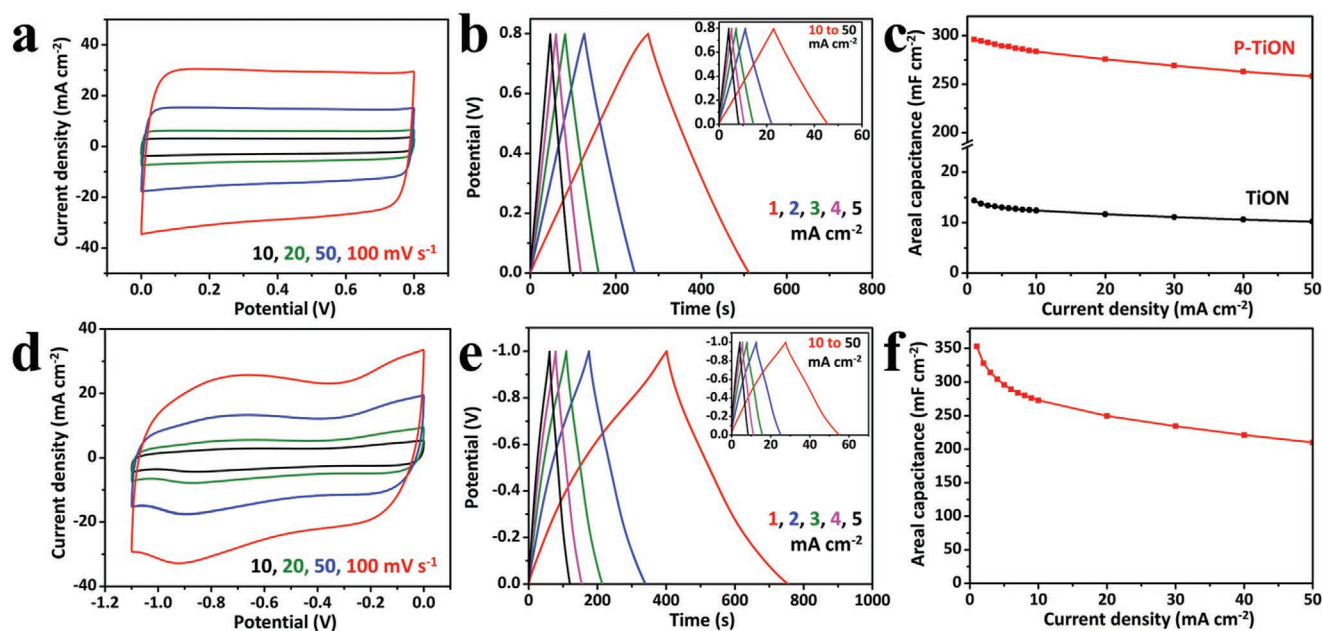


**Figure 3.** Electrochemical performances of P-TiON and VN NW microelectrodes. a) CV curves of P-TiON NW microelectrode at varying scan rates (10, 20, 50, and 100  $\text{mV s}^{-1}$ ). b) GCD curves of P-TiON NW microelectrode at varying current densities from 1 to 5  $\text{mA cm}^{-2}$ , and 10 to 50  $\text{mA cm}^{-2}$  (inset). c) Capacitance retention of P-TiON and TiON NW microelectrodes obtained from GCD versus current density. d) CV curves of VN NW microelectrode at varying scan rates (10, 20, 50, and 100  $\text{mV s}^{-1}$ ). e) GCD curves of VN NW microelectrode at varying current densities from 1 to 5  $\text{mA cm}^{-2}$ , and 10 to 50  $\text{mA cm}^{-2}$  (inset). f) Capacitance retention of VN NW microelectrode obtained from GCD versus current density.

with a high aspect ratio (Figure 2e,f). These NW networks will achieve outstanding electrical conductivity, sufficient ion diffusion pathways, and large surface area. The phases of the TiON and VN (powder samples) are demonstrated through X-ray diffraction (XRD), as shown in Figure S5, Supporting Information. Obviously, the pattern of TiON belongs to TiN (PDF#: 01-087-0632) and TiO (PDF#: 01-077-2170) (Figure S5a, Supporting Information), which is consistent with our reported work,<sup>[37]</sup> indicating the exchange process of N atom at a high temperature of 800 °C. The XRD pattern of VN corresponds well with the standard XRD pattern of VN (PDF#: 03-065-5288) (Figure S5b, Supporting Information). The energy-dispersive X-ray spectroscopy (EDS) mapping results of TiON and P-TiON NW microelectrodes are described in Figures S6 and S7, Supporting Information, respectively. The distribution of Ti and N elements is homogeneous indicating the existence of TiN and the distribution of S element demonstrates the uniform coating of PEDOT. The EDS mapping results of VN NWs exhibit a homogeneous distribution of V and N elements detected from VN (Figure S8, Supporting Information).

The electrochemical measurements of P-TiON and VN NW microelectrodes were conducted with a three-electrode cell using a 2 M LiCl solution. **Figure 3a–c** exhibits the electrochemical performances of the P-TiON and TiON NW microelectrodes. The rectangular shape of cyclic voltammetry (CV) curves (Figure 3a) at scan rates of 10, 20, 50, and 100  $\text{mV s}^{-1}$  (0–0.8 V vs Ag/AgCl), indicating an ideal capacitance behavior of P-TiON NW microelectrode. The galvanostatic charge/discharge (GCD) curves of P-TiON NW microelectrode at different current densities ranging from 1 to 50  $\text{mA cm}^{-2}$  at a potential window between 0 and 0.8 V are displayed in Figure 3b. The

symmetrical triangular shape of the GCD curves of P-TiON NW microelectrode also indicates the excellent electrochemical capacitance which agrees well with the CV results, and the capacitance of the P-TiON NW microelectrode is effectively enhanced by PEDOT coating. As a part of conductive network for P-TiON NW microelectrode, the TiON NW microelectrode exhibits an excellent CV performance, being able to achieve a high scan rate of 10 000  $\text{mV s}^{-1}$  with rectangular CV curves (Figure S9, Supporting Information). Compared with the CV curves of TiON NW microelectrode shown in Figure S10, Supporting Information, the response current increases greatly, and a larger area of CV curves is achieved. Furthermore, the areal capacitances of P-TiON and TiON NW microelectrodes with different current densities are calculated according to the GCD curves (Figure 3c). The P-TiON NW microelectrode has an ultrahigh capacitance of 296  $\text{mF cm}^{-2}$  at a relatively high current density of 1  $\text{mA cm}^{-2}$ , almost 21-fold higher than TiON NW microelectrode of 14  $\text{mF cm}^{-2}$ . When the current density increases by 50-fold of 50  $\text{mA cm}^{-2}$ , the P-TiON and TiON NW microelectrodes show outstanding capacitance retention of 87% and 71%, respectively. The excellent performance of P-TiON NW microelectrode is attributed to the unique structural features, including that 1) the 3D NW network framework has sufficient growth sites for PEDOT; 2) the PEDOT coating with suitable thickness offers abundant space for electrolyte diffusion, and large electrolyte/PEDOT interface; 3) the continuous PEDOT film on the TiON NW network is able to form fast electron transfer pathway, and effectively enhances the electrical conductivity of the microelectrodes (Figure S11, Supporting Information). Figure 3d exhibits the CV curves of VN NW microelectrode under varying scan rates of 10 to 100  $\text{mV s}^{-1}$

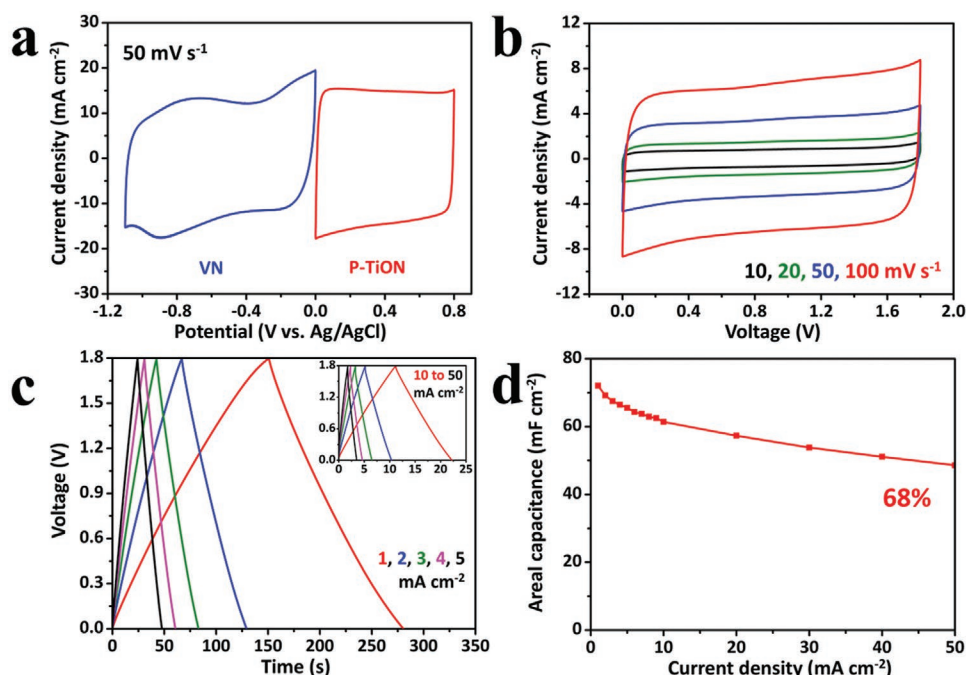


**Figure 4.** Electrochemical performances of P-TiON//VN AMSC. a) CV curves of the P-TiON and VN NW microelectrodes in a three-electrode cell with 2 M LiCl solution. b) CV curves under different scan rates (10, 20, 50, 100  $\text{mV s}^{-1}$ ) with LiCl/PVA electrolyte. c) GCD curves at various current densities ranging from 1 to 5  $\text{mA cm}^{-2}$  and 10 to 50  $\text{mA cm}^{-2}$  (inset). d) Capacitance retention obtained from GCD versus current density.

( $-1.1$  to  $0$  V vs Ag/AgCl), which preserve the same shape with the scan rate increasing, demonstrating the superior capacitive performance. The GCD curves of VN NW microelectrode with quasi-triangle shape are exhibited in Figure 3e, showing a high areal capacitance of  $353 \text{ mF cm}^{-2}$  at a high current density of  $1 \text{ mA cm}^{-2}$ . The areal capacitance of VN NW microelectrode is also exhibited according to the GCD results in Figure 3f, and the high capacitance retention from 1 to  $50 \text{ mA cm}^{-2}$  demonstrates the fast electron/ion transport in the 3D NW network.

Electrochemical performances of all-solid-state P-TiON//VN AMSCs are shown in Figure 4. To investigate the AMSC's working voltage, we combined the CV curves of P-TiON NW cathode and VN NW anode at  $50 \text{ mV s}^{-1}$  in 2 M LiCl electrolyte. As shown in Figure 4a, the operating potential windows of P-TiON and VN NW microelectrodes are  $0$ – $0.8$  V and  $-1.1$ – $0$  V, respectively. Thus, it is anticipated that P-TiON//VN AMSC is stable at a voltage window from  $0$  to  $1.8$  V. To match the charge ( $Q$ ) stored in cathode and anode of AMSCs, the  $Q$  in two electrodes should follow the equation of  $Q^+ = Q^-$ . The values of  $Q^-/Q^+$  of the areal charge of the anode and cathode are exhibited in Figure S12, Supporting Information. The CV profiles of the P-TiON//VN AMSC (LiCl/PVA electrolyte) at varying scan rates are exhibited in Figure 4b. The rectangular CV curves essentially show the same shape at the different scan rates ranging from  $10$  to  $100 \text{ mV s}^{-1}$ , indicating the good capacitive behavior of the AMSC. Figure 4c shows the GCD curves of the AMSC at current densities increasing from  $1$  to  $50 \text{ mA cm}^{-2}$ , exhibiting symmetrical triangle shape. The results demonstrate the excellent capacitive behavior and high reaction reversibility of AMSC. Ultra-small values of internal resistance (IR) drop of AMSC are  $6, 10, 14, 17, 21, 35, 71, 106, 141,$  and  $176 \text{ mV}$  at  $1, 2, 3, 4, 5, 10, 20, 30, 40,$  and  $50 \text{ mA cm}^{-2}$ , respectively, obtained

from GCD profiles (Figure 4c). It indicates the excellent capacitance performance with the high electrical conductivity of the microelectrodes. The areal capacitances of the AMSC at varying current densities according to the GCD results are exhibited in Figure 4d. The AMSC achieves an outstanding areal capacitance of  $72 \text{ mF cm}^{-2}$  at a relatively high current density of  $1 \text{ mA cm}^{-2}$ , and its capacitance retention is  $68\%$  even at an ultrahigh current density of  $50 \text{ mA cm}^{-2}$ . This ultrahigh current density and capacitance retention exceed many reported results (Table S1, Supporting Information). For the cycling performance of the AMSC, it has an excellent capacitance retention of  $86\%$  after  $10\,000$  cycles at  $40 \text{ mA cm}^{-2}$  ( $71\%$ , at  $10 \text{ mA cm}^{-2}$  for  $8000$  cycles), showing great potential for high-reliability MSC (Figure S13, Supporting Information).

Multi-scale hetero integration is the key point for the development of micro energy storage system. Figure 5a schematically illustrates the P-TiON//VN AMSCs in parallel (AMSC-P) and in series (AMSC-S) assembled on a PCB, a light-emitting diode (LED) driven by AMSC-S integrated on the PCB (the circuit design is exhibited in Figure S14, Supporting Information), and an electronic timer driven by an AMSC integrated on the flexible PET bangle. Benefitting from this substrate-free design and construction, the microelectrodes of AMSC-P are capable of stacking precisely along the vertical direction, thus greatly improving its areal mass loading. Meanwhile, each stacked microelectrode has a current collector and the decrease of capacitance is almost negligible. Furthermore, the AMSC-S is able to integrate on the optional position of PCB, improving the designability of the microcircuit. The area of CV curves of AMSC-P is almost twofold of the single AMSC (Figure 5b). Moreover, the shapes of the AMSC-P's voltage profiles are perfectly retained, indicating that the integrated AMSC-P is stable.

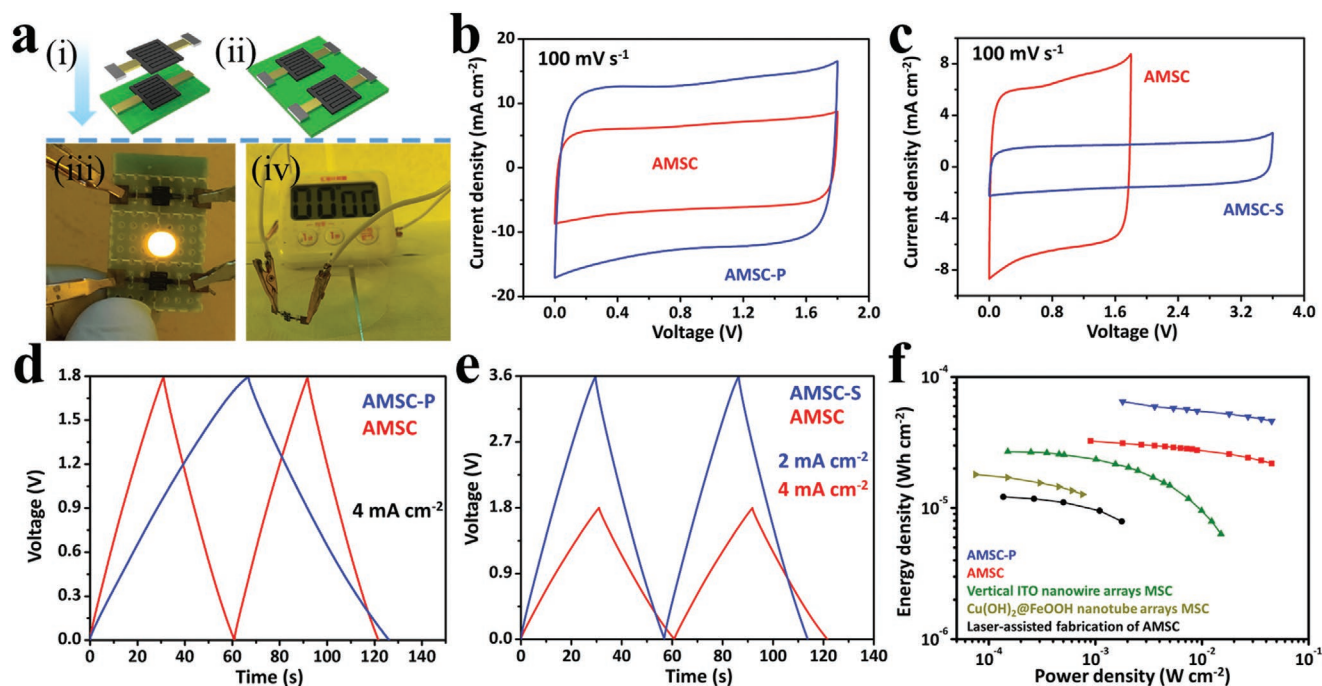


**Figure 5.** a) i) Schematic illustration of the AMSC-P, ii) AMSC-S, iii) a white LED powered by AMSC-S (integrated on a PCB), and iv) an electronic timer driven by an AMSC (integrated on a flexible PET bangle). b) The comparison of CV curves between AMSC-P and AMSC at  $100 \text{ mV s}^{-1}$ . c) The comparison of CV curves of AMSC-S and AMSC at the scan rate of  $100 \text{ mV s}^{-1}$ . d) GCD curves of AMSC-P and AMSC at  $4 \text{ mA cm}^{-2}$ . e) GCD curves of AMSC-S and AMSC at the same current ( $0.56 \text{ mA}$ ). f) Ragone plots showing the areal energy/power densities of AMSC and AMSC-P in comparison with other reported NWs based AMSCs and MSCs.

The CV curves of AMSC-S and single AMSC are exhibited in Figure 5c. The operating voltage of AMSC-S is twofold higher than that of the single AMSC. The GCD curves of AMSC, AMSC-P, and AMSC-S are exhibited in Figure 5d,e. The discharge time of single AMSC is almost half of AMSC-P at the same current density of  $4 \text{ mA cm}^{-2}$ , and its operating voltage is half of AMSC-S under the same current of  $0.56 \text{ mA}$ . Ragone plot (Figure 5f) shows the comparison of the areal energy/power densities of AMSC, AMSCs-P, and some previously reported high-performance symmetrical/asymmetric MSCs. The AMSC delivers an energy density of  $32.4 \mu\text{Wh cm}^{-2}$  (at  $0.9 \text{ mW cm}^{-2}$ ), and a high energy density of  $21.9 \mu\text{Wh cm}^{-2}$  is maintained at a high power density of  $45 \text{ mW cm}^{-2}$ . Moreover, The AMSC-P shows an energy density of  $64.9 \mu\text{Wh cm}^{-2}$  at a power density of  $0.18 \text{ mW cm}^{-2}$ . Even at a high power density of  $45 \text{ mW cm}^{-2}$ , an energy density of  $46 \mu\text{Wh cm}^{-2}$  is remained. These outstanding electrochemical performances are superior to those of many reported MSCs based on NW electrodes, including the polypyrrole@multi-walled CNT cathode based AMSCs;<sup>[16]</sup> the  $\text{Cu}(\text{OH})_2$ @FeOOH nanotube arrays based MSC;<sup>[40]</sup> and the vertical ITO NW arrays@ $\text{MnO}_2$  MSC.<sup>[41]</sup> The high areal energy and power densities of the AMSC could be ascribed to the outstanding performances of network microelectrodes constructed by high-mass-loading interwoven NWs, which achieve continuous electron/ion transport pathway and large specific surface area (the thickness of the microelectrodes and the Ragone plot of volumetric energy/power densities are exhibited in Figures S15 and S16, Supporting Information, respectively).

In summary, an all-solid-state P-TiON//VN AMSC, constructed by interwoven NW network microelectrodes is

fabricated, achieving high energy/power density. The high-mass-loading interwoven NW network of the microelectrodes has continuous electron/ion transport pathway and large specific surface area. The assembled AMSC shows a superior areal capacitance of  $72 \text{ mF cm}^{-2}$ , a high energy density of  $32.4 \mu\text{Wh cm}^{-2}$  (at  $0.9 \text{ mW cm}^{-2}$ ), and an outstanding power density of  $45 \text{ mW cm}^{-2}$  (at  $21.9 \mu\text{Wh cm}^{-2}$ ). In addition, the substrate-free NW AMSC is highly applicable in the microelectronic system. These high-performance AMSCs by the convenient and rapid process have a great potential for commercial applications in microdevices, and the proposed procedure has great promise in many high-performance micro energy storage devices with active NWs. Moreover, the substrate-free microelectrodes by mass production are able to provide a low-cost and convenient research platform for the development and characterization of microelectrodes.

## Experimental Section

**Synthesis of  $\text{H}_2\text{Ti}_3\text{O}_7$  NWs:**  $\text{H}_2\text{Ti}_3\text{O}_7$  NWs were synthesized by a reported hydrothermal method.<sup>[37]</sup> Briefly,  $\text{TiO}_2$  (anatase) (2 g) was added into NaOH solution (30 mL, 15 M) under magnetic stirring for 1 h. Then, the suspension was transferred to a Teflon-lined stainless steel autoclave and heated in an oven at  $180 \text{ }^\circ\text{C}$  for 72 h. After cooling down to room temperature, the product was stirred in HCl (0.1 M) solution for 24 h. Finally, the material obtained after filtration was rinsed several times with deionized (DI) water and alcohol, followed by drying at  $70 \text{ }^\circ\text{C}$  for 12 h.

**Synthesis of  $\text{VO}_x$  NWs:**  $\text{VO}_x$  NWs were hydrothermally synthesized according to a reported method.<sup>[31]</sup>  $\text{NH}_4\text{VO}_3$  (0.324 g) was dissolved in a mixed solution (50 mL) of DI water and ethanol (v/v: 9/1). After the

pH value of the solution was tuned to  $\approx 2.0$  by HCl, the solution was poured into a 50 mL Teflon-lined autoclave. The autoclave was heated at 160 °C for 12 h, and then naturally cooled down to room temperature. The green  $\text{VO}_x$  NWs were rinsed three times with DI water, followed by drying at 70 °C for 12 h.

**Fabrication of P-TiON NW Microelectrodes:** P-TiON NW microelectrodes were fabricated through an EP process. Briefly,  $\text{H}_2\text{Ti}_3\text{O}_7$  NWs (20 mg) were dispersed in alcohol (20 mL) with  $\text{Mg}(\text{NO}_3)_2$  (5 mg) as a surfactant. After ultrasonication for 1 h, the color of the EP suspension became white. An industrially processed Ti interdigital microelectrode with four fingers and a Pt foil were employed as negative and positive electrodes, respectively. EP was conducted on the Ti microelectrode at a constant voltage of 30 V for 5 min. Afterward, all the fingers of Ti microelectrode turned to white and a fluffy layer of  $\text{H}_2\text{Ti}_3\text{O}_7$  NWs containing ethanol was physically absorbed on the microelectrode. After drying at 80 °C with an electrode holder on the heating stage, a dense  $\text{H}_2\text{Ti}_3\text{O}_7$  NWs film was obtained. Then, the  $\text{H}_2\text{Ti}_3\text{O}_7$  NW microelectrodes were transferred to a combustion boat. By annealing at 800 °C for 3 h in  $\text{NH}_3$  flow, the TiON NW microelectrodes were fabricated. The P-TiON NW microelectrodes were fabricated through a CV EDP with a CHI760D electrochemical workstation under a typical three-electrode electrochemical system. The TiON NW microelectrode was employed as a working electrode directly, a Pt foil was employed as a counter electrode, and a saturated Ag/AgCl was employed as a reference electrode. The typical deposition was performed in a mixed solution of EDOT (100  $\mu\text{L}$ ), SDS (50 mg), and DI water (20 mL) with the potential window of 0–1.2 V (vs Ag/AgCl) at 50  $\text{mV s}^{-1}$  for 90 cycles. The P-TiON NW microelectrode was rinsed with DI water, then dried at 70 °C for 30 min.

**Fabrication of VN NW Microelectrodes:** The VN NW microelectrodes were fabricated by a similar method as that of TiON NW microelectrodes. First,  $\text{VO}_x$  NWs (20 mg) were dispersed in alcohol (20 mL) with  $\text{Mg}(\text{NO}_3)_2$  (5 mg) as a surfactant. After ultrasonication for 1 h, the EP suspension turned to dark green. EP was conducted on the Ti microelectrodes at a constant voltage of 60 V for 4 min to deposit  $\text{VO}_x$  NWs. After drying, the same annealing conditions were adopted, and VN NW microelectrodes were achieved.

**Fabrication of All-Solid-State P-TiON/VN AMSC:** All-solid-state P-TiON/VN AMSC was fabricated by fixing of P-TiON and VN NW microelectrodes directly onto a PCB, which were aligned with an optical microscope. The LiCl/PVA gel electrolyte was obtained after continuously stirring LiCl (3 g) and PVA (3 g) in DI water (30 mL) at 90 °C for 2 h until the solution was clear, and then cooled down naturally. The gel electrolyte was utilized to coat the asymmetric microelectrodes, and the P-TiON/VN all-solid-state AMSC was assembled.

**Materials and Devices Characterization:** SEM images were obtained with a JEOL JSM-7100F SEM at an acceleration voltage of 20.0 kV. The EDS results were recorded by an Oxford IE250 system. The XRD patterns were recorded using a D8 DISCOVER X-ray diffractometer with Cu  $K\alpha$  radiation ( $\lambda = 1.5418 \text{ \AA}$ ).

**Electrochemical Measurements:** The CV and GCD results were recorded by a CHI760D to examine the electrochemical performances of TiON NW microelectrode, P-TiON NW microelectrode, VN NW microelectrode, and the AMSCs. The EIS tests of TiON and P-TiON NW microelectrodes were conducted by an Autolab 302N. The CV and GCD tests of TiON, P-TiON, and VN NW microelectrodes were measured by a three-electrode system. The electrochemical performances of AMSCs were measured by a two-electrode system.

The areal capacitances ( $C_{\text{half}}$ ) of P-TiON and VN NW microelectrodes are according to the following equation:

$$C_{\text{half}} = \frac{I\Delta t}{A\Delta V} \quad (1)$$

where  $I$ ,  $\Delta t$ ,  $\Delta V$ , and  $A$  are the discharge current, the discharge time after IR drop, the potential window, and the print area of half of the full device (0.07  $\text{cm}^2$ , Figure S1a,b, Supporting Information), respectively.

The areal charge ( $Q$ ) of P-TiON and VN NW microelectrodes are calculated using the following equations:<sup>[42]</sup>

$$Q = C_{\text{half}} \times \Delta V \quad (2)$$

where  $C_{\text{half}}$  is the areal capacitances of P-TiON or VN NW microelectrodes, the  $\Delta V$  is the potential window.

The areal capacitance ( $C_{\text{full}}$ ) of P-TiON/VN all-solid-state AMSC is according to the following equations:<sup>[43]</sup>

$$C_{\text{full}} = \frac{I\Delta t}{A\Delta V} \quad (3)$$

where  $I$ ,  $\Delta t$ ,  $\Delta V$ , and  $A$  are the discharge current, the discharge time after IR drop, the voltage window, and the print area of the full device (0.14  $\text{cm}^2$ , Figure S1a,b, Supporting Information), respectively.

The areal energy density ( $E_a$ ) and areal power density ( $P_a$ ) are calculated using the following equation:<sup>[44]</sup>

$$E_a = \frac{C_{\text{full}}\Delta V^2}{7200} \quad (4)$$

$$P_a = \frac{E_a}{\Delta t} \times 3600 \quad (5)$$

where  $C_{\text{full}}$  is the areal specific capacitance calculated through GCD curves,  $\Delta V$  corresponds to the voltage window, and  $\Delta t$  refers to the discharge time.

## Supporting Information

Supporting Information is available from the Wiley Online Library or from the author.

## Acknowledgements

W.Y. and Y.Z. contributed equally to this work. This work was supported by the National Natural Science Foundation of China (51521001, 51802239), the National Key Research and Development Program of China (2016YFA0202604), Foshan Xianhu Laboratory of the Advanced Energy Science and Technology Guangdong Laboratory (XHT2020-003, XHT2020-005), the Fundamental Research Funds for the Central Universities (2020111011GX, 20201VB057, 20191VB054, 2019111062JL, 20201VA068), the National Innovation and Entrepreneurship Training Program for College Students (20191049701030), the Program of Introducing Talents of Discipline to Universities (B17034), the Yellow Crane Talent (Science & Technology) Program of Wuhan City.

## Conflict of Interest

The authors declare no conflict of interest.

## Keywords

asymmetric microsupercapacitors, electrophoresis, interwoven nanowire networks, titanium oxynitride, vanadium nitride

Received: June 7, 2020

Revised: August 22, 2020

Published online:

[1] D. Qi, Y. Liu, Z. Liu, L. Zhang, X. Chen, *Adv. Mater.* **2017**, *29*, 1602802.

[2] Z. L. Wang, *Adv. Mater.* **2012**, *24*, 280.

[3] M. Beidaghi, Y. Gogotsi, *Energy Environ. Sci.* **2014**, *7*, 867.

- [4] N. Choudhary, C. Li, J. Moore, N. Nagaiyah, L. Zhai, Y. Jung, J. Thomas, *Adv. Mater.* **2017**, *29*, 1605336.
- [5] N. A. Kyeremateng, T. Brousse, D. Pech, *Nat. Nanotechnol.* **2017**, *12*, 7.
- [6] Z. Hao, L. Xu, Q. Liu, W. Yang, X. Liao, J. Meng, X. Hong, L. He, L. Mai, *Adv. Funct. Mater.* **2019**, *29*, 1808470.
- [7] J. H. Pikul, H. Gang Zhang, J. Cho, P. V. Braun, W. P. King, *Nat. Commun.* **2013**, *4*, 1732.
- [8] Y. He, P. Zhang, M. Wang, F. Wang, D. Tan, Y. Li, X. Zhuang, F. Zhang, X. Feng, *Mater. Horiz.* **2019**, *6*, 1041.
- [9] Z. S. Wu, K. Parvez, S. Li, S. Yang, Z. Liu, S. Liu, X. Feng, K. Mullen, *Adv. Mater.* **2015**, *27*, 4054.
- [10] X. Tian, M. Shi, X. Xu, M. Yan, L. Xu, A. Minhas-Khan, C. Han, L. He, L. Mai, *Adv. Mater.* **2015**, *27*, 7476.
- [11] M. Beidaghi, C. Wang, *Electrochim. Acta* **2011**, *56*, 9508.
- [12] F. Li, J. Wang, L. Liu, J. Qu, Y. Li, V. K. Bandari, D. Karnaushenko, C. Becker, M. a. Faghih, T. Kang, S. Baunack, M. Zhu, F. Zhu, O. G. Schmidt, *Adv. Sci.* **2019**, *6*, 1901051.
- [13] Y. Zhong, M. Yang, X. Zhou, Z. Zhou, *Mater. Horiz.* **2015**, *2*, 553.
- [14] H. Sun, J. Zhu, D. Baumann, L. Peng, Y. Xu, I. Shakir, Y. Huang, X. Duan, *Nat. Rev. Mater.* **2019**, *4*, 45.
- [15] M. Tahir, L. He, W. A. Haider, W. Yang, X. Hong, Y. Guo, X. Pan, H. Tang, Y. Li, L. Mai, *Nanoscale* **2019**, *11*, 7761.
- [16] J. Gao, C. Shao, S. Shao, F. Wan, C. Gao, Y. Zhao, L. Jiang, L. Qu, *Small* **2018**, *14*, 1801809.
- [17] D. Pech, M. Brunet, H. Durou, P. Huang, V. Mochalin, Y. Gogotsi, P. L. Taberna, P. Simon, *Nat. Nanotechnol.* **2010**, *5*, 651.
- [18] D. Kim, J. Yun, G. Lee, J. S. Ha, *Nanoscale* **2014**, *6*, 12034.
- [19] J. O. Omale, R. Rupp, P. V. Velthem, V. V. Kerckhoven, V. A. Antohe, A. Vlad, L. Piraux, *Energy Storage Mater.* **2019**, *21*, 77.
- [20] J. Lin, C. Zhang, Z. Yan, Y. Zhu, Z. Peng, R. H. Hauge, D. Natelson, J. M. Tour, *Nano Lett.* **2013**, *13*, 72.
- [21] P. Huang, D. Pech, R. Lin, J. K. McDonough, M. Brunet, P.-L. Taberna, Y. Gogotsi, P. Simon, *Electrochem. Commun.* **2013**, *36*, 53.
- [22] L. Mai, X. Tian, X. Xu, L. Chang, L. Xu, *Chem. Rev.* **2014**, *114*, 11828.
- [23] G. Zhou, L. Xu, G. Hu, L. Mai, Y. Cui, *Chem. Rev.* **2019**, *119*, 11042.
- [24] B. Gao, X. Li, K. Ding, C. Huang, Q. Li, P. K. Chu, K. Huo, *J. Mater. Chem. A* **2019**, *7*, 14.
- [25] B. Anasori, M. R. Lukatskaya, Y. Gogotsi, *Nat. Rev. Mater.* **2017**, *2*, 16098.
- [26] C. Zhu, P. Yang, D. Chao, X. Wang, X. Zhang, S. Chen, B. K. Tay, H. Huang, H. Zhang, W. Mai, H. J. Fan, *Adv. Mater.* **2015**, *27*, 4566.
- [27] X. Lu, T. Liu, T. Zhai, G. Wang, M. Yu, S. Xie, Y. Ling, C. Liang, Y. Tong, Y. Li, *Adv. Energy Mater.* **2014**, *4*, 1300994.
- [28] B. Anothumakkool, R. Soni, S. N. Bhange, S. Kurungot, *Energy Environ. Sci.* **2015**, *8*, 1339.
- [29] Z. Su, C. Yang, C. Xu, H. Wu, Z. Zhang, T. Liu, C. Zhang, Q. Yang, B. Li, F. Kang, *J. Mater. Chem. A* **2013**, *1*, 12432.
- [30] L. Mai, F. Dong, X. Xu, Y. Luo, Q. An, Y. Zhao, J. Pan, J. Yang, *Nano Lett.* **2013**, *13*, 740.
- [31] X. Lu, M. Yu, T. Zhai, G. Wang, S. Xie, T. Liu, C. Liang, Y. Tong, Y. Li, *Nano Lett.* **2013**, *13*, 2628.
- [32] X. Xiao, X. Peng, H. Jin, T. Li, C. Zhang, B. Gao, B. Hu, K. Huo, J. Zhou, *Adv. Mater.* **2013**, *25*, 5091.
- [33] Q. Zhang, X. Wang, Z. Pan, J. Sun, J. Zhao, J. Zhang, C. Zhang, L. Tang, J. Luo, B. Song, Z. Zhang, W. Lu, Q. Li, Y. Zhang, Y. Yao, *Nano Lett.* **2017**, *17*, 2719.
- [34] Y. Yang, L. He, C. Tang, P. Hu, X. Hong, M. Yan, Y. Dong, X. Tian, Q. Wei, L. Mai, *Nano Res.* **2016**, *9*, 2510.
- [35] Q. Jiang, N. Kurra, M. Alhabeb, Y. Gogotsi, H. N. Alshareef, *Adv. Energy Mater.* **2018**, *8*, 1703043.
- [36] W. Yang, L. He, X. Tian, M. Yan, H. Yuan, X. Liao, J. Meng, Z. Hao, L. Mai, *Small* **2017**, *13*, 1700639.
- [37] J. Dong, Y. Jiang, Q. Li, Q. Wei, W. Yang, S. Tan, X. Xu, Q. An, L. Mai, *J. Mater. Chem. A* **2017**, *5*, 10827.
- [38] Z.-S. Wu, S. Pei, W. Ren, D. Tang, L. Gao, B. Liu, F. Li, C. Liu, H.-M. Cheng, *Adv. Mater.* **2009**, *21*, 1756.
- [39] J. Zhang, Y. Li, Y. Zhang, X. Qian, R. Niu, R. Hu, X. Zhu, X. Wang, J. Zhu, *Nano Energy* **2018**, *43*, 91.
- [40] J.-Q. Xie, Y.-Q. Ji, J.-H. Kang, J.-L. Sheng, D.-S. Mao, X.-Z. Fu, R. Sun, C.-P. Wong, *Energy Environ. Sci.* **2019**, *12*, 194.
- [41] J. Du, Y. Zhao, Z. Zhang, X. Mu, X. Jiang, B. Huang, Y. Zhang, S. Zhang, Z. Zhang, E. Xie, *J. Mater. Chem. A* **2019**, *7*, 6220.
- [42] X. Cheng, J. Zhang, J. Ren, N. Liu, P. Chen, Y. Zhang, J. Deng, Y. Wang, H. Peng, *J. Phys. Chem. C* **2016**, *120*, 9685.
- [43] K. Shen, J. Ding, S. Yang, *Adv. Energy Mater.* **2018**, *8*, 1800408.
- [44] L. Li, J. Zhang, Z. Peng, Y. Li, C. Gao, Y. Ji, R. Ye, N. D. Kim, Q. Zhong, Y. Yang, H. Fei, G. Ruan, J. M. Tour, *Adv. Mater.* **2016**, *28*, 838.